The sun's meridional circulation and interior magnetic field

Jeremy McCaslin Pascale Garaud

University of California Santa Cruz, ISIMA, 2010

Abstract

This effort explores the fundamental dynamics of a solar model such as that of Gough and McIntyre[1]. The interaction of meridional flows downwelling from the convection zone into the radiative interior with a confined interior magnetic field is explored through a simple Cartesian model and linearized governing equations. Semi-analytical solutions provide insight into these dynamics that have implications for magnetic confinement and gyroscopic pumping, as well as for stellar mixing.

Introduction

Helioseismic observations[2, 3, 4] suggest that the solar convection zone exhibits a strong level of differential rotation, whereby the rotation period of the polar regions is about 25% - 30% longer than the equatorial regions. Meanwhile, the radiative interior of the sun undergoes nearly uniform rotation. These two regions are separated by a thin shear-layer called the tachocline[5]. How is the differential rotation in the convection zone prevented from propagating into the radiative interior? This has been a long-standing question in solar physics. There is no strictly hydrodynamical model that could sustain this configuration. The standard explanation for the uniform rotation of the radiative interior is the presence of a large-scale primordial magnetic field through Ferraro isorotation[1]. However, this in turn leads to the issue of magnetic confinement, as the field would otherwise naturally diffuse radially outward. Large-scale meridional flows that downwell from the convection zone into the radiative interior provide the mechanism for field confinement. The Coriolis force associated with the zonal (longitudinal) flows perpetually "pumps" the convection zone fluid, and maintains a quasi-steady circulation, poleward near the surface[6, 7]. The amplitude and spatial distribution of these meridional flows deeper in the convection zone remains essentially unknown, as the sensitivity of helioseismic methods rapidly drops below the surface. As a result, the question of whether some of the pumped mass flux actually penetrates into the underlying radiative zone is still open, despite its obvious importance for mixing of chemical species[8, 9], and its presumed role in the dynamical balance of the solar interior[1, 10, 11, 12] and some models of the solar dynamo (see [13] for a review).

In this paper, we construct a linearized, Cartesian toy model to gain insight into the interaction of downwelling meridional flows with an interior, poloidal magnetic field. The work stems from the hydrodynamic model of [14], extending it to the magnetic case. First, we lay out the Cartesian model and the governing equations for our simplified system. Next, we discuss the numerical results of the unstratified, Boussinesq case and derive analytical scalings that match the numerical solutions. Lastly, we discuss the effect of a stratified interior, relating our results to the recent work of [15].

A Cartesian model

Model setup

As a first approach to gain fundamental understanding of meridional circulation interacting with an interior magnetic field, a simplified Cartesian model is sufficient and greatly simplifies the required algebra. For non-dimensionalization of the equations, distances are normalized by the solar radius $R_\odot$ and velocities to $R_\odot\Omega_\odot$, where $\Omega_\odot$ is the mean solar rotation rate. As can be seen in figure 1, our Cartesian (x, y, z) coordinate system is chosen so that x represents the azimuthal coordinate ϕ (with $0 < x < 2\pi$), and y is the negative of the co-latitude such that $y = 0$ and $y = \pi$ correspond to the poles while $y = \pi/2$ corresponds to the equator. The radial direction corresponds to z in our coordinate system, and is such that $0 < z < 1$

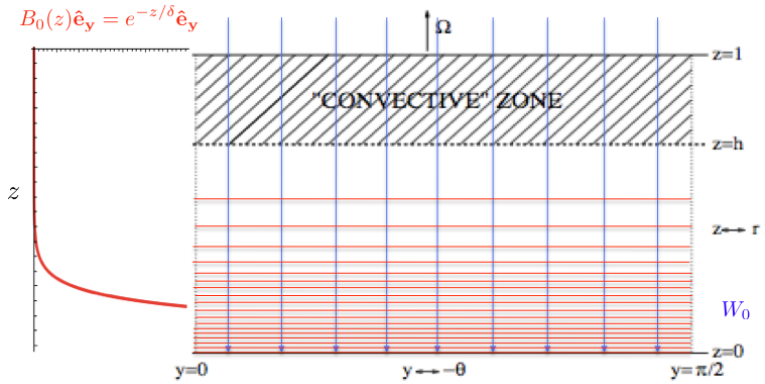

Figure 1: Schematic of the Cartesian model. The shaded region designates the convection zone, where forcing is applied. The system is π-periodic in the y direction. The dotted line at $z = h$ corresponds to the base of the convection zone. Red lines indicate the exponentially decaying background magnetic field, blue lines indicate the uniform downwelling flow used to balance diffusion of this field (see main text for details).

due to normalization. As can be seen by the shaded region, the convection zone represents the region where $z > h$, while the radiative interior corresponds to $0 < z < h$. The assumed background state of the problem is clearly visible in figure 1, which will be discussed in the next section.

Model equations

The full set of (non-dimensional) governing equations for this system are, respectively, conservation of momentum and thermal energy, along with the induction equation, mass conservation equation and the solenoidal condition on the magnetic field:

$$\frac{\partial \mathbf{U}}{\partial t} + \mathbf{U}\cdot\nabla\mathbf{U} + 2\hat{\mathbf{e}}_\mathbf{z}\times\mathbf{U} = -\nabla P + T\hat{\mathbf{e}}_\mathbf{z} + \bar{V}_A^2\,\mathbf{J}\times\mathbf{B} + E_\nu\nabla^2\mathbf{U} \tag{1}$$

$$\frac{\partial T}{\partial t} + \mathbf{U}\cdot\nabla T + b^2\mathbf{U}\cdot\hat{\mathbf{e}}_\mathbf{z} = E_\kappa\nabla^2 T \tag{2}$$

$$\frac{\partial \mathbf{B}}{\partial t} = \nabla\times(\mathbf{U}\times\mathbf{B}) + Rm^{-1}\nabla^2\mathbf{B} \tag{3}$$

$$\nabla\cdot\mathbf{U} = 0 \tag{4}$$

$$\nabla\cdot\mathbf{B} = 0\,, \tag{5}$$

where U is the velocity, B is the magnetic field, J is current, P is pressure, and T is the temperature perturbation. Using a dynamic scaling for pressure and normalizing the temperature perturbations to $R_\odot\bar{T}_z$ (the background temperature difference across the box), the non-dimensional parameters introduced are

$$\bar{V}_A^2 = \frac{B_0^2}{4\pi\rho_0 R_\odot^2\Omega_\odot^2}\,, \quad \text{the Alfvén parameter;} \tag{6}$$

$$E_\nu = \frac{\nu}{R_\odot^2\Omega_\odot}\,, \quad \text{the Ekman number;} \tag{7}$$

$$b = \frac{N}{\Omega_\odot}\,, \quad \text{the frequency ratio;} \tag{8}$$

$$E_\kappa = \frac{E_\nu}{\mathrm{Pr}}\,, \quad \text{the thermal diffusion parameter;} \tag{9}$$

$$Rm = \frac{R_\odot^2\Omega_\odot}{\eta}\,, \quad \text{the magnetic Reynolds number;} \tag{10}$$

where B_0 and ρ_0 are unit field and density respectively, ν is the viscosity, κ is the thermal diffusivity, and η is the magnetic diffusivity. N is the Brunt-Väisälä frequency and $\mathrm{Pr} = \nu/\kappa_T$ is the conventional Prandtl number (ratio of viscosity to thermal diffusivity). The Alfvén parameter $\bar{V}_A^2$ is the square of the ratio of the Alfvén speed to the characteristic speed $R_\odot\Omega_\odot$, and the frequency ratio b is simply the non-dimensional buoyancy frequency.

The buoyancy frequency N characterizes the transition between the model convective and radiative zones, which goes from zero in the convection zone ($z > h$) to nonzero in the interior ($z < h$). In order to model this behavior, we define the non-dimensional buoyancy frequency to be of the form

$$b(z) = \frac{b_{rz}}{2}\left\{1 + \tanh\left(\frac{h-z}{\Delta}\right)\right\}\,, \tag{11}$$

where b_{rz} is constant and characterizes the strength of stratification. Note that $b \approx b_{rz}$ in the interior. The lengthscale Δ can be thought of as the thickness of the "overshoot" region

near the base of the convection zone, but in practice is mostly used to ensure continuity and smoothness of the background state through the tanh function.

As previously mentioned, we are considering an axially symmetric, steady-state problem, and therefore set $\partial/\partial x = \partial/\partial t = 0$. We further simplify our model by making assumptions about the nonlinear terms in the momentum and energy equations (1) and (2). Within the stably stratified radiation zone, $\mathbf{U}\cdot\nabla\mathbf{U}$ and $\mathbf{U}\cdot\nabla T$ are assumed to be negligible. In the convection zone, on the other hand, it is known that anisotropic turbulent stresses drive the differential rotation. In order to model this simply and appropriately for our linear approach, we replace the divergence of the stresses with a linear relaxation toward the observed convection zone profile:

$$\mathbf{u}\cdot\nabla\mathbf{u} \longrightarrow \mathbf{F}_{turb} = \frac{\mathbf{u} - u_{cz}(y,z)\hat{\mathbf{e}}_{\mathbf{x}}}{\tau} \tag{12}$$

where u_{cz} models the observed azimuthal velocity profile in the solar convection zone and τ is the relaxation timescale which can be viewed as a dimensionless convective turnover timescale. This prescription is similar to that used in [16]. We adopt the profile

$$u_{cz}(y,z) = \frac{U_0(z)}{2}\left\{1 + \tanh\left(\frac{z-h}{\Delta}\right)\right\} e^{iky} = \hat{u}_{cz}e^{iky}\,, \tag{13}$$

where

$$U_0(z) = U_0(h) + S(z-h) \tag{14}$$

and $k = 2$ to due to equatorial symmetry. The function $U_0(z)$ governs the nature of the forcing in the convection zone, where setting $U_0(h) = 0$ implies that the forcing goes to zero at the base of the convection zone. S is the parameter that governs the imposed vertical shear in the azimuthal direction. Note that the amplitude of the forcing is somewhat irrelevant due to the linearity of the problem.

As for $b(z)$ and $\hat{u}_{cz}(z)$ in equations (11) and (13), the dimensionless relaxation timescale τ can be modeled as

$$\tau^{-1}(z) = \frac{1}{2\,\tau_c}\left\{1 + \tanh\left(\frac{z-h}{\Delta}\right)\right\}. \tag{15}$$

For simplicity, we assume that τ_c is constant while keeping in mind that it varies by as much as 3 orders of magnitude in the real solar convection zone.

Turbulent convection efficiently mixes heat in the convection zone, thus the asphericity in the temperature profile is negligible in this region. Therefore we can model the advection of temperature fluctuations by the fluid as an enhanced diffusivity:

$$\mathbf{u}\cdot\nabla T \longrightarrow -D(z)\nabla^2 T\,. \tag{16}$$

Again, we use the tanh function to model the diffusion coefficient:

$$D(z) = \frac{D_0}{2}\left\{1 + \tanh\left(\frac{z-h}{\Delta}\right)\right\}, \tag{17}$$

where D_0 governs the amplitude of this enhanced diffusion. We will assume that $D_0 \gg 1$, meaning that the dimensionless diffusion timescale $1/D_0$ is much smaller than other typical timescales in the physical system.

We have simplified equations (1)-(5) with our steady state and axial symmetry assumptions, as well as our models for the nonlinear advection terms in the momentum and thermal energy equation. We now proceed to linearize the remaining terms (the Lorentz force and the field advection in the induction equation) by assuming that the velocity and magnetic fields are

$$\mathbf{U} = \mathbf{W_0} + \mathbf{u} = W_0 \hat{\mathbf{e}}_\mathbf{z} + \begin{Bmatrix} u \\ v \\ w \end{Bmatrix} \tag{18}$$

$$\mathbf{B} = \mathbf{B_0} + \mathbf{b} = B_0(z) \hat{\mathbf{e}}_\mathbf{y} + \begin{Bmatrix} b_x \\ b_y \\ b_z \end{Bmatrix} , \tag{19}$$

where the perturbations $\{u, v, w, b_x, b_y, b_z\}$ (along with T in the momentum and energy equations (1) and (2)) are to be solved for. The Lorentz force in (1) and the induction equation (3) must be carefully expanded, and only terms linear in the perturbations are kept. Assuming the perturbations to be periodic in y with an amplitude that depends on z, i.e. seeking solutions of the form

$$q = \hat{q}(z)\, e^{iky} , \tag{20}$$

our equations generate a system of ODEs for the perturbation amplitudes $\hat{q}$. This system of ODEs can be solved in a straightforward manner, upon one last clarification: the dimensionless background magnetic field is defined as

$$B_0(z) = e^{-z/\delta} , \tag{21}$$

where δ corresponds to the thickness of the magnetic boundary layer (refer to figure 1). Note that the previously defined B_0 constant is the dimensional value of $B_0(0)$. In order to balance the diffusion of this field, W_0 is introduced. This balance is seen clearly from the y component of the induction equation:

$$\frac{\partial}{\partial z}(W B_0) = Rm^{-1} \nabla^2 (B_0(z) + b_y) , \tag{22}$$

where $W = W_0(z) + \hat{w}(z) e^{iky}$ and $b_y = \hat{b}_y e^{iky}$. We can eliminate terms not proportional to e^{iky} if

$$W_0(z) B_0(z) = Rm^{-1} \frac{dB_0}{dz} , \tag{23}$$

assuming the arbitrary integration constant to be zero. Using (21), this implies that

$$W_0 = -\frac{1}{Rm\delta} \quad \text{or} \quad |W_0| = \frac{\eta}{\delta} , \tag{24}$$

which is the expected downwelling velocity required for confinement. Note that an exponential choice of $B_0(z)$ allows for a constant W_0, making it unnecessary to modify v in satisfaction of mass continuity.

Based on all previously listed assumptions, the equations governing the perturbation amplitudes become:

$$-2\hat{v} = ik\bar{V}_A^2\hat{b}_x e^{-z/\delta} + E_\nu\left(\frac{d^2\hat{u}}{dz^2} - k^2\hat{u}\right) - \frac{\hat{u}-\hat{u}_{cz}}{\tau(z)} \tag{25}$$

$$2\hat{u} = -ik\hat{p} - \frac{1}{\delta}\bar{V}_A^2\hat{b}_z e^{-z/\delta} + E_\nu\left(\frac{d^2\hat{v}}{dz^2} - k^2\hat{v}\right) - \frac{\hat{v}}{\tau(z)} \tag{26}$$

$$\frac{d\hat{p}}{dz} - \hat{T} = \frac{1}{\delta}\bar{V}_A^2\hat{b}_y e^{-z/\delta} + \bar{V}_A^2\left(ik\hat{b}_z - \frac{d\hat{b}_y}{dz}\right)e^{-z/\delta} + E_\nu\left(\frac{d^2\hat{w}}{dz^2} - k^2\hat{w}\right) - \frac{\hat{w}}{\tau(z)} \tag{27}$$

$$ik\hat{u}e^{-z/\delta} - W_0\hat{b}_x' = -Rm^{-1}\left(\frac{d^2\hat{b}_x}{dz^2} - k^2\hat{b}_x\right) \tag{28}$$

$$\frac{W_0}{R_\odot\Omega_\odot}\frac{d\hat{b}_y}{dz} + (\hat{w}e^{-z/\delta})' = Rm^{-1}\left(\frac{d^2\hat{b}_y}{dz^2} - k^2\hat{b}_y\right) \tag{29}$$

$$\frac{ikW_0}{R_\odot\Omega_\odot}\hat{b}_y + ik\hat{w}e^{-z/\delta} = -Rm^{-1}\left(\frac{d^2\hat{b}_z}{dz^2} - k^2\hat{b}_z\right) \tag{30}$$

$$\hat{w} = \frac{1}{b^2(z)}\left[E_\kappa + D(z)\right]\left(\frac{d^2\hat{T}}{dz^2} - k^2\hat{T}\right) \tag{31}$$

$$ik\hat{v} + \frac{d\hat{w}}{dz} = 0 \tag{32}$$

$$ik\hat{b}_y + \frac{d\hat{b}_z}{dz} = 0\,. \tag{33}$$

Note that $\hat{p}$ in equations (26) and (27) now incorporates both the thermodynamic pressure as well as the magnetic pressure caused by the background field. We proceed to solve our system of ODEs numerically using a packaged two-point boundary value algorithm available in MATLAB called bvp4c. Analytical scalings for the perturbations are derived for various regions of the domain. These semi-analytical results reveal characteristic behavior of the downwelling flows that we believe to be relevant to the regime of the solar tachocline.

Results

The Unstratified Case

We begin our analysis with the unstratified case by setting $b_{rz} = 0$. The constraint will be lifted in the next section, but the essence of the problem can be shown in the absence of

stratification. In the unstratified, purely hydrodynamic study of [14], it was demonstrated that downwelling meridional flows in the convection zone only penetrate into the radiation zone in the presence of a no-slip boundary condition at the interior of the sun. As artificial as this boundary condition may be, the implications are very important: there must be stresses present in the radiation zone in order for the Taylor-Proudman constraint to be broken and allow downwelling flows to return to the convection zone. If stress-free conditions are used at the bottom of the domain, meridional flows do not penetrate into the interior, but rather return at the base of the convection zone, i.e. where there is a mechanical pathway that allows them to do so. This is illustrated in figure 2, which shows that the flow amplitude in the radiation zone scales with E_ν if the lower boundary condition is stress-free.

The Lorentz Force

The motivation for this work is based on the findings discussed above. The presence of a confined magnetic field within the solar interior adds a Lorentz force in the momentum equation, thus providing the mechanical pathway required for the penetration of meridional circulation into the solar interior. It will also be seen that Lorentz forces will allow for larger mass fluxes (more penetration) than solely the shear stresses confined to a very thin Ekman Layer, in the purely hydrodynamic case. This accommodation of greater mass fluxes has implications for stellar mixing (i.e., lithium stars[15]).

In the absence of stratification, the thermal energy equation (31) and $\hat{T}$ in equation (27) can be neglected. As a first check for the unstratified case, we solve the case for either $B_0 = 0$ or $\bar{V}_A^2 = 0$ (no Lorentz force), as seen in figure 2. We obtain the purely hydrodynamic,

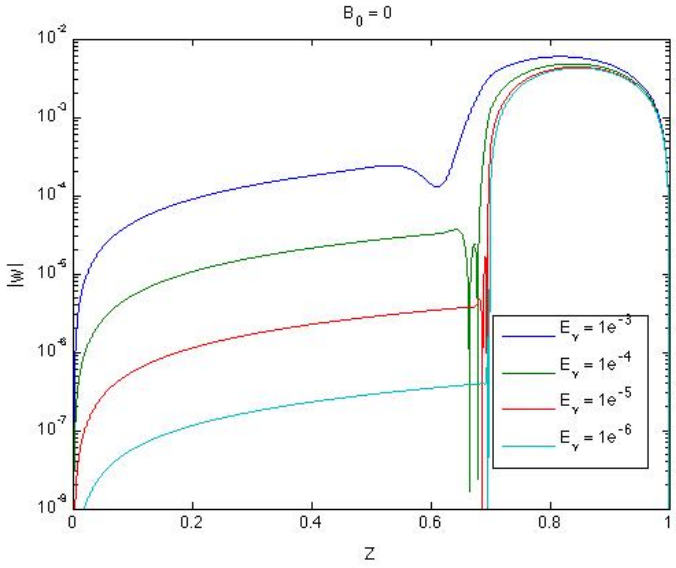

Figure 2: The unstratified case with $B_0 = 0$. The lower boundary is stress-free ($\partial_z \hat{u} = \partial_z \hat{v} = 0$) and impermeable ($\hat{w} = 0$). The perturbation $\hat{w}$ scales with E_ν in the interior.

unstratified solution of [15], where the downwelling perturbation $\hat{w}$ scales with the Ekman

number in the radiation zone (for the stress-free boundary condition). After reproducing the hydrodynamic solution in the case of no magnetic field, we set the Lorentz parameter $\bar{V}_A^2$ to a nonzero value. It is clear in figure 3 that when Lorentz forces dominate viscous

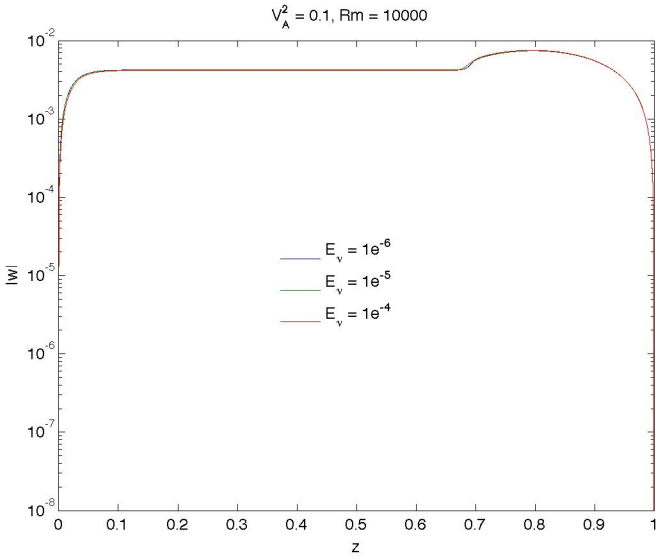

Figure 3: A small, nonzero Lorentz force eliminates the scaling of $\hat{w}$ with E_ν in the interior.

stresses in the momentum equation radically different dynamics are observed. In particular, the dependence of the solution on E_ν dissapears. We study this effect more systematically in figure 4 by gradually increasing the strength of the Lorentz force. A layer develops within the interior where the downwelling perturbation $\hat{w}$ decays exponentially. Further increasing the Lorentz force causes this magnetically dominated region to span the entire radiation zone, eventually suppressing the flows in the convection zone if the Lorentz force becomes strong enough (see figure 4). Because our model assumes all perturbations to be axisymmetric in x, we can define the velocity streamfunction Ψ and the magnetic potential a and use them to visualize streamlines and magnetic field lines. The magnetically dominated region discussed above is clearly visible, as shown in figure 5. False color images of the azimuthal velocity and magnetic field perturbations are also shown. We see 3 main regions: the convection zone, where dynamics are dominated by the convection stresses and drive pumping, a magnetic free region in Taylor-Proudman balance and, finally a magnetically dominated region in uniform rotation.

Because the background field $B_0(z)$ has no Lorentz force, its only physical effect is magnetic pressure, which has been included in the thermodynamic pressure. It is therefore important to note at this point that due to linearization, the Alfvén parameter $\bar{V}_A^2$ and the magnetic Reynolds number Rm are physically coupled. This can be seen mathematically by folding the Alfvén parameter into the magnetic perturbations, $\bar{b}_i = \bar{V}_A^2 \hat{b}_i$, and recasting the

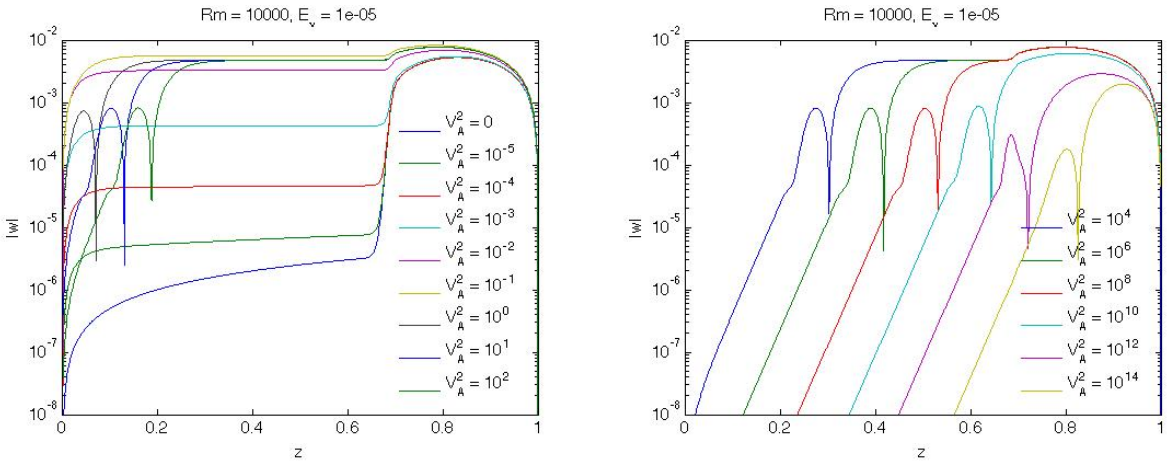

(a) Formation of magnetically dominated region.

(b) Magnetically dominated region spreading across radiation zone.

Figure 4: The magnetically dominated region spreads across the radiation zone as the Lorentz force is increased, eventually suppressing the circulation in the convection zone.

momentum and induction equations:

$$2\hat{\mathbf{e}}_\mathbf{z} \times \mathbf{u} = -\nabla P + \mathbf{j} \times \mathbf{B} + E_\nu \nabla^2 \mathbf{u} - \frac{\mathbf{u} - u_{cz}\hat{\mathbf{e}}_\mathbf{x}}{\tau} \tag{34}$$

$$\nabla \times (\mathbf{U} \times \mathbf{B}) = -\Lambda^{-1} \nabla^2 \mathbf{B}\,, \tag{35}$$

where the dimensionless parameter Λ is the Elsasser number, defined as

$$\Lambda = \bar{V}_A^2\, Rm = \frac{B_0^2}{4\pi\rho_0\eta\Omega_\odot} \tag{36}$$

in this case. For negligible viscosity in the presence of Lorentz forces (as was shown in figure 3), Λ is becomes the only dimensionless parameter for this unstratified case. The physical reasoning for this goes as follows: as the background field itself has no Lorentz force, increasing the strength of the Lorentz force means increasing the interaction of the velocity perturbations with the background field (the LHS of the equation (35)). Through the induction equation, this has the equivalent effect of increasing the effective magnetic Reynolds number. If Rm is very large, there is strong interaction between the field and the flow, but if Rm is small the field diffuses away and the flow does not "feel" that it is there. The exact same behavior can be obtained by decreasing or increasing η of course. This mathematical and physical reasoning is evident in figure 6, where increasing Rm (decreasing η) has the same effect as increasing $\bar{V}_A^2$.

Structure of the Magnetically Dominated Region

As the background magnetic state corresponds to the imposed $B_0(z) = e^{-z/\delta}$, it is important to explore the effect that δ has on the behavior of the solution. The parameter δ governs

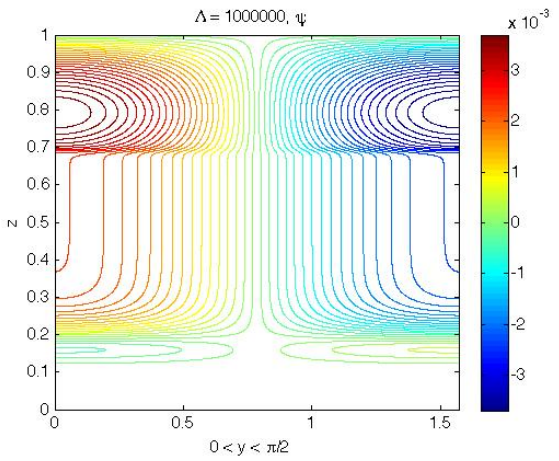

(a) Streamlines reveal where the flow is forced to turn around.

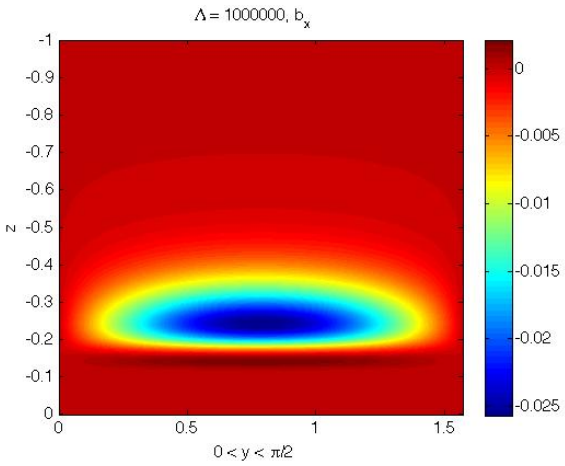

(b) The azimuthal component of the magnetic perturbation is strongest near the turn-around region.

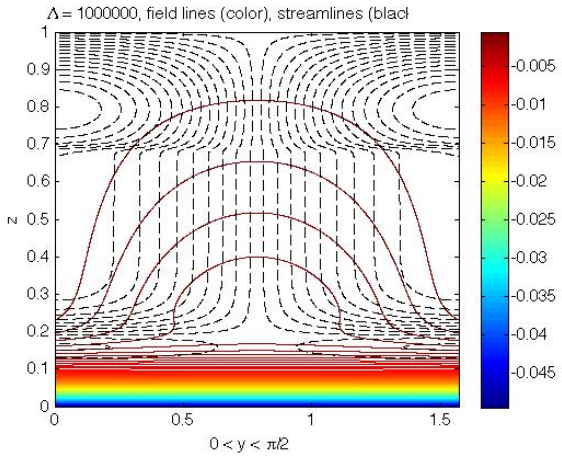

(c) Velocity streamlines and magnetic field lines.

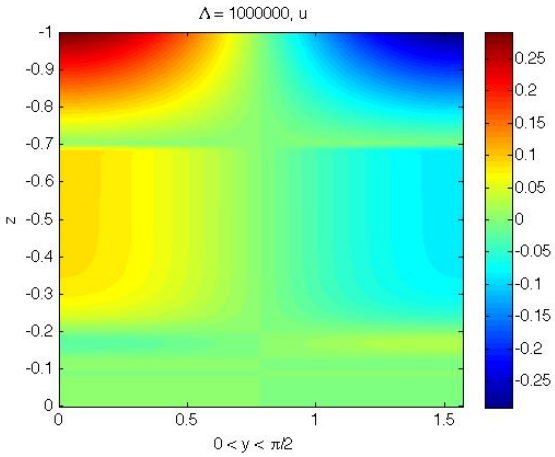

(d) The azimuthal velocity shows uniform rotation in the magnetically dominated region and Taylor-Proudman rotation above up to the base of the convection zone.

Figure 5: (a) provides visualization of the magnetically dominated region; (b) demonstrates the azimuthal component of the magnetic perturbation; (c) shows Ψ = constant lines superimposed on magnetic field lines; (d) demonstrates how azimuthal velocity is affected by the magnetic field.

how much of the normalized solar radius is magnetically dominated, for a given interior field strength as measured by Λ. Figure 7(a) demonstrates the effect that increasing δ has on the perturbation $\hat{w}$. It is also clear from figure 7(a) that δ has a slight effect on the magnitude of the downwelling flow, but more interestingly it also affects the thickness of the transition between the magnetically dominated region and the region of constant $\hat{w}$ (this region will be mentioned in the next section). For the value of $\delta = 0.2$, the transition region is becoming

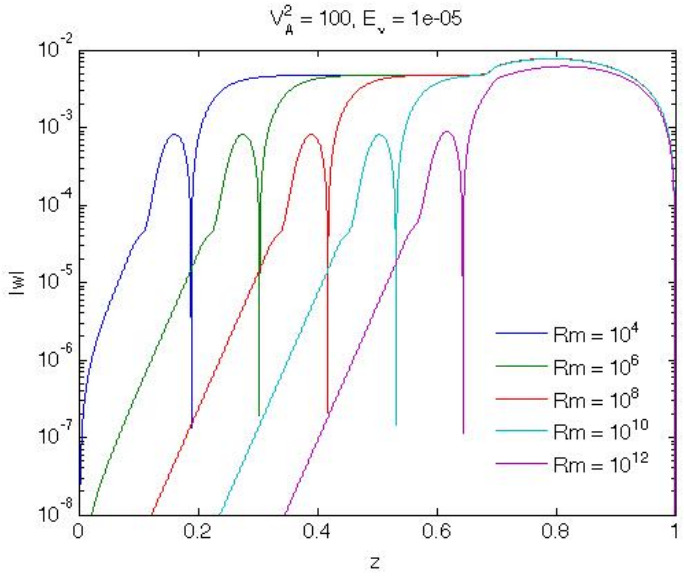

Figure 6: Decreasing η has the same effect as increasing the strength of the Lorentz force (figure 4).

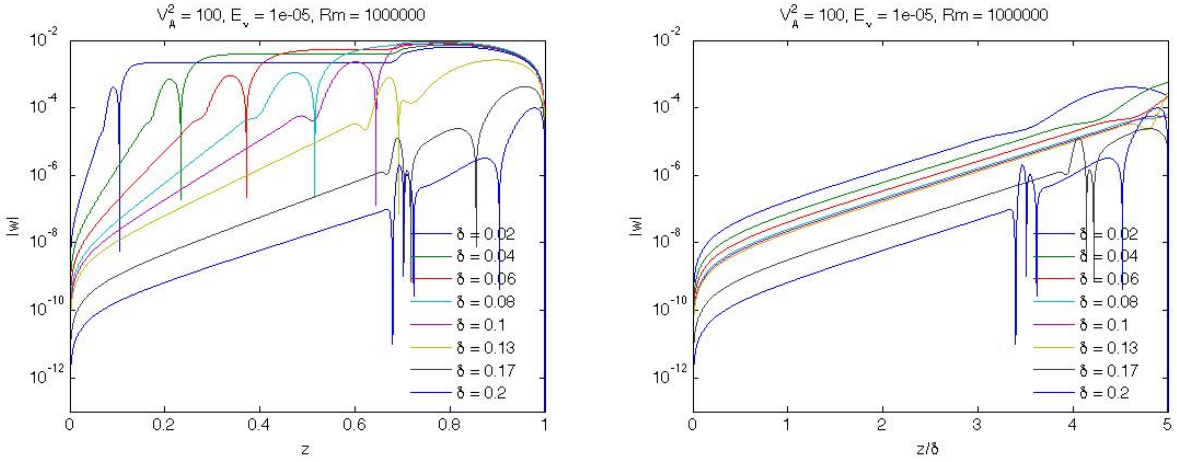

(a) Varying δ affects the thickness of the magnetically dominated region, the thickness of the transition region, and the magnitude of $\hat{w}$.

(b) Plotting $\hat{w}$ verse z/δ suggests an exponential decay that is independent of δ.

Figure 7: The effect of δ on the perturbation $\hat{w}$.

somewhat difficult to resolve. This is not largely important, as having a δ of 20 % of the normalized solar radius does not have physical relevance. If we plot $\hat{w}$ as a function of z/δ rather than z, we see in figure 7(b) that there is a suggested universal exponential profile for $\hat{w}$ that is a function of z/δ only.

Analytical Perturbation Scalings

As was demonstrated in figure 7(b), the exponential scaling of $\hat{w}$ seems to exhibit a universal solution in the magnetically dominated region, for a range of δ. Because viscosity is negligible, and we are in the radiative interior where there is no forcing, we neglect viscous stresses and the forcing terms. The system of equations (25)-(30) becomes

$$-2\hat{v} = ik\bar{V}_A^2\hat{b}_x e^{-z/\delta} \tag{37}$$

$$2\hat{u} = -ik\hat{p} - \frac{1}{\delta}\bar{V}_A^2\hat{b}_z e^{-z/\delta} \tag{38}$$

$$\frac{d\hat{p}}{dz} = \frac{1}{\delta}\bar{V}_A^2\hat{b}_y e^{-z/\delta} + \bar{V}_A^2\left(ik\hat{b}_z - \frac{d\hat{b}_y}{dz}\right)e^{-z/\delta} \tag{39}$$

$$ik\hat{u}e^{-z/\delta} - W_0\hat{b}_x' = -Rm^{-1}\left(\frac{d^2\hat{b}_x}{dz^2} - k^2\hat{b}_x\right) \tag{40}$$

$$\frac{W_0}{R_\odot\Omega_\odot}\frac{d\hat{b}_y}{dz} + (\hat{w}e^{-z/\delta})' = Rm^{-1}\left(\frac{d^2\hat{b}_y}{dz^2} - k^2\hat{b}_y\right) \tag{41}$$

$$\frac{ikW_0}{R_\odot\Omega_\odot}\hat{b}_y + ik\hat{w}e^{-z/\delta} = -Rm^{-1}\left(\frac{d^2\hat{b}_z}{dz^2} - k^2\hat{b}_z\right). \tag{42}$$

This system of ODEs can be solved analytically for $\hat{w}$ to yield the form

$$\hat{w}'' - 2\hat{w}' = \underbrace{\frac{4}{k^3\delta^4\Lambda^2}e^{4z/\delta}}_{\Pi(z)}\mathcal{L}(\hat{w}), \tag{43}$$

where $\mathcal{L}(\hat{w})$ is a linear, differential operator containing first and higher order derivatives of $\hat{w}$ only. If we consider the limit where the coefficient $\Pi(z) \ll 1$, then the solution $\hat{w}$ must be proportional to $e^{2z/\delta}$. This is in fact the behavior of $\hat{w}$ we find numerically in the magnetically dominated region, as visible in figure 8(a) for a range of δ. This scaling begins to deviate slightly for $\delta = 0.3$ (30 % of the normalized solar radius), which is not of concern.

Considering the case when $\Pi(z) \sim 1$, the exponentially decaying solution is no longer valid and the solution changes to $\hat{w}$ = constant (as clearly seen in figure 7(a) for a variety of δ). Although it is not clearly obvious from equation (43) why $\hat{w}$ becomes constant, one can see that a trivial solution is $\hat{w}' = 0$ (therefore $\mathcal{L}(\hat{w}) = 0$).

Similar scalings can be derived for all of the remaining perturbation quantities $\hat{q}$:

$$\hat{q}'' - n\,\hat{q}' = \Pi_q\,\mathcal{L}(\hat{q}), \tag{44}$$

where Π_q is the coefficient corresponding to the perturbation q, and n is given for each perturbation in table 1. This means that

$$\hat{q} \sim e^{nz/\delta}, \tag{45}$$

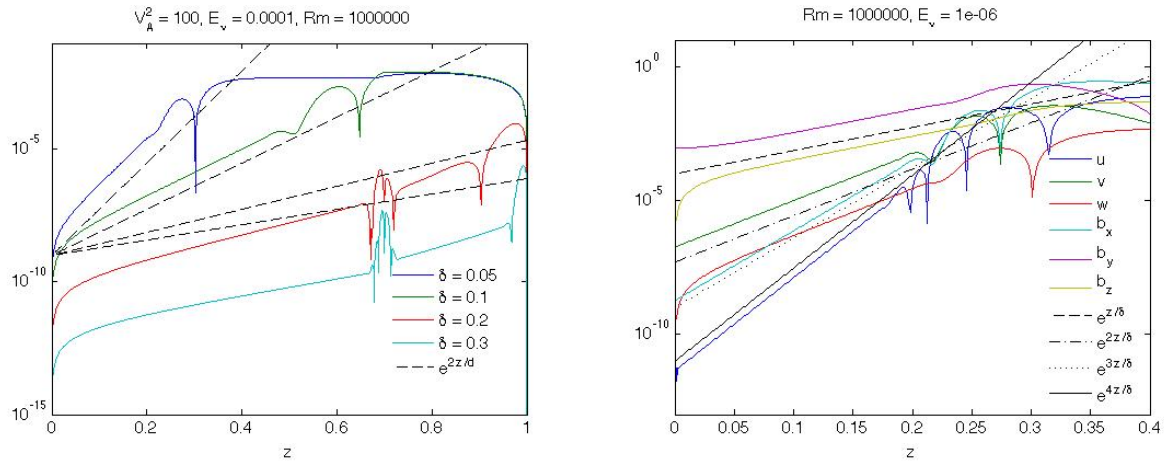

(a) The scaling $\hat{w} \sim e^{2z/\delta}$ is valid for a range of δ.

(b) The exponential scalings for all of the perturbations.

Figure 8: Analytical scalings for the velocity and magnetic field perturbations.

Table 1: Values of n for each perturbation.

n	$\hat{q}$
1	$\hat{b}_y$, $\hat{b}_z$
2	$\hat{v}$, $\hat{w}$
3	$\hat{b}_x$
4	$\hat{u}$

and the corresponding scalings can be seen graphically in figure 8(b).

Going back to the case of $\hat{w}$ the point z where $\Pi(z) \sim 1$, should correspond to the position of the transition point between the exponentially decaying and $\hat{w} =$ constant regions. Solving the equation

$$\Pi(z) = \frac{4}{k^3\delta^4\Lambda^2} e^{4z/\delta} = 1 \tag{46}$$

yields

$$z = \frac{\delta}{4} \log\left(\frac{k^3\delta^4\Lambda^2}{4}\right) . \tag{47}$$

This prediction for the position of the transition point is compared with the numerical solution in figure 9 and shows excellent agreement.

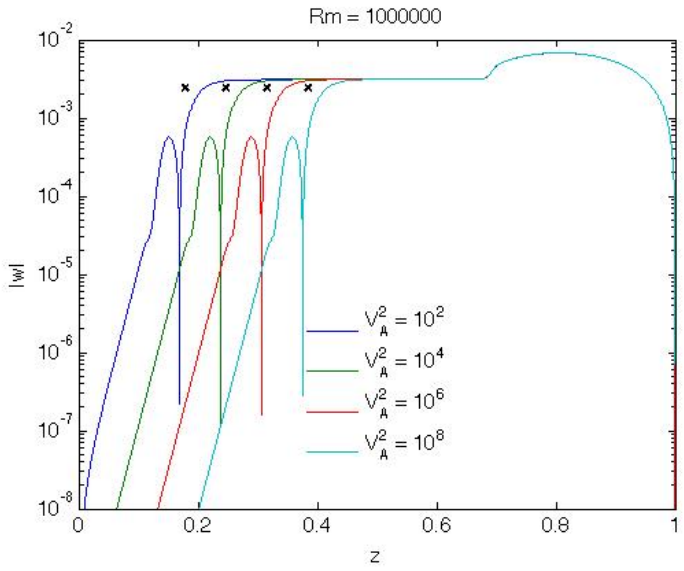

Figure 9: Prediction of transition location as a function of Λ, based on equation (47).

The Stratified Case

In the previous section, we discussed the effect of the Lorentz force, as measured by the Elsasser number Λ, on the character of the downwelling perturbation $\hat{w}$. We also looked at how the structure of the magnetically dominated region depends on δ and developed analytical solutions for the exponential decay of the perturbations in this region. In this section, we increase the physical realism of the model by adding stratification to the radiative interior ($b_{rz} \neq 0$).

Regimes of Stratification

In order to study the effect of stratification, we return to the full system of equations (25)-(33). Before doing so, we review the recent work of Garaud and Bodenheimer[15], where the role of stratification is explored for the purely hydrodynamic case. The relevance of this work will be clear when we look at the results. In [15], three regimes are found, depending on the strength of stratification (as measured by b_{rz}):
(1) the *unstratified* regime, where the downwelling circulation is indistinguishable from the case of no stratification;
(2) the *weakly* stratified regime, where the downwelling perturbation remains constant with depth and scales as an Eddington-Sweet velocity;
(3) the *strongly* stratified regime, where the flows decay exponentially with depth below the convection zone:

$$\hat{w} \sim e^{\pm\sigma(z-h)}\,, \quad \pm\sigma = \pm\sqrt{\mathrm{Pr}}\frac{b_{rz}}{2}k\,. \tag{48}$$

In figure 10, our numerical solution of the full system is shown, for $\hat{w}$, for a fixed Elsasser number and increasing values of b_{rz}. The magnetically dominated region is clearly visible, while the region above exhibits the the three regimes discussed earlier. The values of $b_{rz} =$

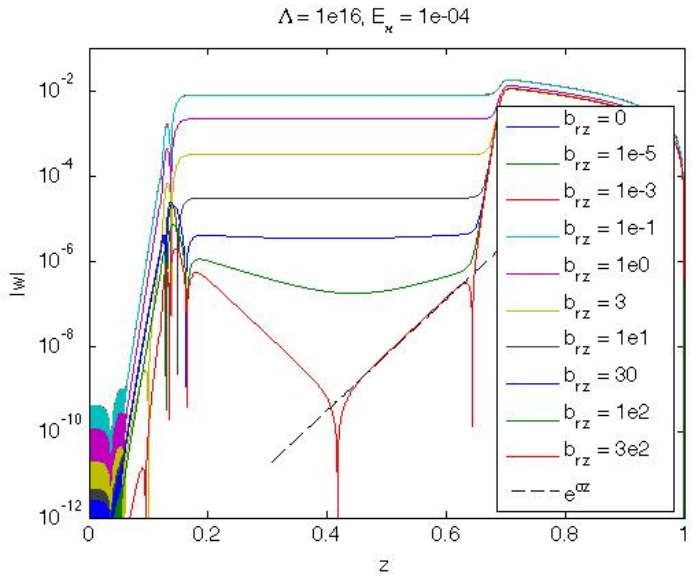

Figure 10: Demonstration of the three regimes for stratification.

10^{-5}, 10^{-3}, and 10^{-1} correspond to the green, red, and cyan lines, respectively; and each of these lines fall directly on type of the purple line of $b_{rz} = 0$. This indicates that these values of b_{rz} fall into the *unstratified* regime. Similarly, the values of $b_{rz} = 1$, 3, and 10 (purple, yellow, and black) show that $\hat{w}$ is still constant in the intermediate region, with a value which follows roughly the Eddington-Sweet scaling ($\hat{w} \propto \frac{\Omega_\odot}{NE_\kappa}$) and therefore belong to the *weakly* stratified regime. The figure indicates that the values of $b_{rz} = 30$ and 100 (blue and green) transition from the weakly to *strongly* stratified regime, which is characterized well by the red line, corresponding to $b_{rz} = 300$. The dashed line displays the exponential decay $\hat{w} \sim e^{\sigma z}$ found in [15].

Varying Field Strength with Stratification

We have seen that adding stratification changes the scaling of the velocity in the magnetic-free region that lies in between the magnetically dominated region and the unstratified convection zone, according to the three regimes found in [15]. How does this behavior interact with the effect of increasing the Elsasser number Λ? Numerical results suggest that stratification and field strength are decoupled in the sense that increasing the field strength lengthens the magnetically dominated region (as shown in the absence of stratification); while increasing the stratification affects the magnetic-free region, according to the three regimes of [15]. This behavior is evident in figure 11. Within each plot, different colors indicate different values of b_{rz}; while figure 11(a) corresponds to $\Lambda = 10^7$ and figure 11(b) to

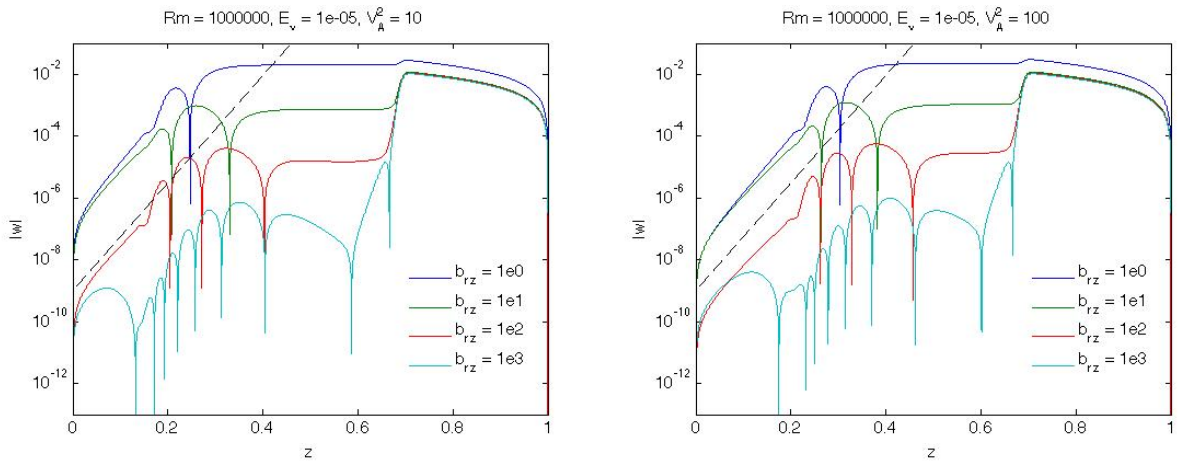

(a) Varying b_{rz}, $\Lambda = 10^7$.

(b) Varying b_{rz}, $\Lambda = 10^8$.

Figure 11: Different colors within each plot show different values of b_{rz}; different figures show different values of Λ.

$\Lambda = 10^8$. The dashed line demonstrates the $\hat{w} \sim e^{2z/\delta}$ scaling in the magnetically dominated region. It is clear that increasing Λ by an order of magnitude merely increases the size of the magnetically dominated region, while the amplitude of the downwelling flows in the magnetic-free region remains controlled only by the level of stratification.

Conclusion

The meridional circulation driven by the observed differential rotation profile in the solar convection zone may penetrate into the solar interior, having implications for both magnetic confinement as well as stellar mixing. In fact, the standard Gough and McIntyre model[1] requires an interior field to explain the interesting configuration of the sun, for which there is no purely hydrodynamic explanation. In this work, a uniform downwelling flow has been used to balance the diffusion of the background magnetic field, and a linear analysis has been performed in a simplified Cartesian geometry. The perturbations to both the magnetic and velocity fields have been solved for numerically, and analytical scalings for the solutions provided. The intent of this work is to gain fundamental understanding into the interaction of penetrating meridional circulation with a confined, interior poloidal field.

In the first part of this paper, we used the simplifying assumption of an unstratified solar interior to add to the work of [14], demonstrating that in order for meridional circulation to downwell into the solar interior, there must be forces present in order to break the Taylor-Proudman constraint within the interior, allowing the flows to return to the convection zone. The presence of Lorentz forces provide the necessary mechanical pathway for this to occur. Lorentz forces also accomodate higher mass fluxes and are more relevant to the solar interior than the viscous stresses of [14]. Interestingly, the magnitude of the downwelling

flow in the magnetic-free region does not know about the size of the magnetically dominated

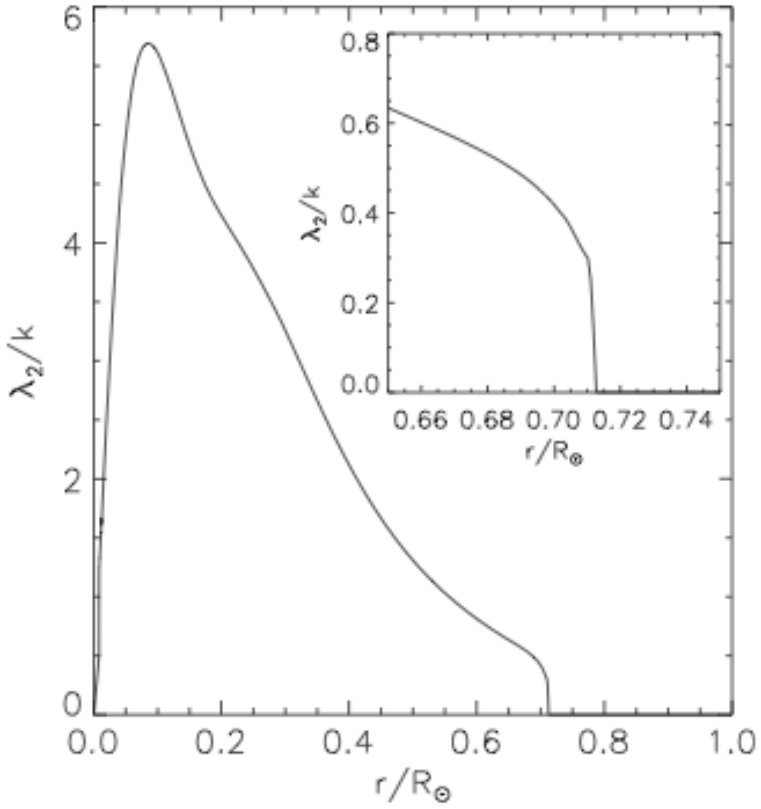

Figure 12: The relevance of the solar tachocline to the weakly stratified regime, taken from [14].

region below, which is a function of the Elsasser number. This parameter merely governs the point at which the downwelling flows turn over and return the convection zone. Analytically deriving exponential scalings for the perturbations in the magnetically dominated region, the point at which $\hat{w}$ transitions from magnetically dominated to magnetic-free can be solved for and is in good agreement with numerical solutions.

The second half of the paper works toward increasing the physical realism of the model by adding stratification to the solar interior. We find that field strength and stratification are decoupled from one another, in that increasing the field strength has the exact same effect that it did in the absence of stratification. The scaling of $\hat{w}$ in the magnetic-free region is governed by the level of stratification and can be categorized into three regimes: unstratified, weakly stratified, and strongly stratified. This result is in accordance with the recent findings of [15]. In short, this work has found two regions of interest:
(1) the magnetically dominated region, for which the same treatment as the unstratified case applies for the weakly stratified regime (which we believe is relevant to the solar tachocline). Analytical scalings have been developed that predict the behavior of this region.
(2) the magnetic-free region, for which the scaling of $\hat{w}$ is dictated by the level of stratification

and falls into the three regimes of [15]. Figure 12 demonstrates the relevance of the solar tachocline to the weakly stratified regime, for which our analytical scalings hold.

Although this model is helpful as a first step in understanding the interaction of downwelling meridional circulation with an interior magnetic field, the background flow confining the field is not physical. Rather, the downwelling perturbations that we solve for in this model are what confine the field. In future work, we seek a way to link these perturbations to the downwelling background flow that we have imposed; this would essentially close the model and provide insight toward meridional circulation that confines an interior, primordial field within the solar radiation zone.

References

[1] D. O. Gough and M. E. McIntyre, "Inevitability of a magnetic field in the sun's radiative interior," *Nature*, vol. 394, no. 6695, pp. 755–757, 1998.

[2] M. J. Thompson, J. Toomre, E. R. Anderson, H. M. Antia, G. Berthomieu, D. Burtonclay, S. M. Chitre, J. Christensen-Dalsgaard, T. Corbard, M. DeRosa, C. R. Genovese, D. O. Gough, D. A. Haber, J. W. Harvey, F. Hill, R. Howe, S. G. Korzennik, A. G. Kosovichev, J. W. Leibacher, F. P. Pijpers, J. Provost, E. J. Rhodes, J. Schou, T. Sekii, P. B. Stark, and P. R. Wilson, "Differential rotation and dynamics of the solar interior," *Science*, vol. 272, pp. 1300–1305, May 1996.

[3] A. G. Kosovichev, J. Schou, P. H. Scherrer, R. S. Bogart, R. I. Bush, J. T. Hoeksema, J. Aloise, L. Bacon, A. Burnette, C. D. Forest, *et al.*, "Structure and rotation of the solar interior: initial results from the MDI medium-l program," *Solar Physics*, vol. 170, no. 1, p. 4361, 1997.

[4] J. Schou, H. M. Antia, S. Basu, R. S. Bogart, R. I. Bush, S. M. Chitre, J. Christensen-Dalsgaard, M. P. Mauro, W. A. Dziembowski, A. Eff-Darwich, *et al.*, "Helioseismic studies of differential rotation in the solar envelope by the solar oscillations investigation using the michelson doppler imager," *The Astrophysical Journal*, vol. 505, p. 390, 1998.

[5] E. A. Spiegel and J. P. Zahn, "The solar tachocline," *Astronomy and Astrophysics*, vol. 265, p. 106114, 1992.

[6] P. H. Haynes, M. E. McIntyre, T. G. Shepherd, C. J. Marks, and K. P. Shine, "On the 'Downward control' of extratropical diabatic circulations by Eddy-Induced mean zonal forces.," *Journal of Atmospheric Sciences*, vol. 48, pp. 651–680, Feb. 1991.

[7] P. Garaud, "Magnetic confinement of the solar tachocline," *The solar tachocline*, p. 147, 2007.

[8] M. Pinsonneault, "Mixing in stars," *Annual Review of Astronomy and Astrophysics*, vol. 35, pp. 557–605, 1997.

[9] J. R. Elliott and D. O. Gough, "Calibration of the thickness of the solar tachocline," *The Astrophysical Journal*, vol. 516, pp. 475–481, May 1999.

[10] M. E. McIntyre, *The Solar Tachocline, ed.* DW Hughes, R. Rosner, & NO Weiss (Cambridge: Cambridge Univ. Press), 2007.

[11] P. Garaud, *The Solar Tachocline, ed.* DW Hughes, R. Rosner, & NO Weiss (Cambridge: Cambridge Univ. Press), 2007.

[12] P. Garaud and J. Garaud, "Dynamics of the solar tachocline - II. the stratified case," *Monthly Notices of the Royal Astronomical Society*, vol. 391, pp. 1239–1258, Dec. 2008.

[13] P. Charbonneau, "Dynamo models of the solar cycle," *Living Reviews in Solar Physics*, vol. 2, p. 2, June 2005.

[14] P. Garaud and L. A. Arreguin, "ON THE PENETRATION OF MERIDIONAL CIRCULATION BELOW THE SOLAR CONVECTION ZONE. II. MODELS WITH CONVECTION ZONE, THE TAYLOR-PROUDMAN CONSTRAINT, AND APPLICATIONS TO OTHER STARS," *The Astrophysical Journal*, vol. 704, no. 1, pp. 1–16, 2009.

[15] P. Garaud and P. Bodenheimer, "GYROSCOPIC PUMPING OF LARGE-SCALE FLOWS IN STELLAR INTERIORS AND APPLICATION TO LITHIUM-DIP STARS," *The Astrophysical Journal*, vol. 719, no. 1, pp. 313–334, 2010.

[16] F. P. Bretherton and A. E. Spiegel, "The effect of the convection zone on solar Spin-Down," *The Astrophysical Journal*, vol. 153, p. L77, Aug. 1968.